Effect of molecular film thickness on thermal conduction across solid-film interfaces

Zhi Liang and Hai-Lung Tsai[*]

Department of Mechanical and Aerospace Engineering, Missouri University of Science and Technology,
400 W. 13th Street, Rolla, Missouri 65409, USA

The Brownian motion and aggregation of particles in nanofluids often lead to the formation of solid-film-solid structures. The molecular thin film confined between nanoparticles may have non-negligible effects on thermal conduction among nanoparticles. Using nonequilibrium molecular dynamics simulations, we study thermal conduction across the Ag particle-Ar thin-film interface. If the film contains only one molecular layer, we find that the solid-film interfacial thermal resistance R_{SF} is about 1 order of magnitude smaller than the solid-liquid (bulk) interfacial thermal resistance R_{SL}. If there are two or more molecular layers in the film, it is shown that R_{SF} increases rapidly toward R_{SL} as film thickness increases. By comparing the vibrational density of states of Ag atoms and Ar molecules in the film, we demonstrate that the low thermal resistance in the monolayer film case is caused by the resonant thermal transport between Ag particles and Ar thin films.

I. INTRODUCTION

The solid-liquid interfacial thermal resistance R_{SL} has been extensively studied experimentally and theoretically in the past decade [1–6] since R_{SL} is a critical physical property for understanding the microscopic thermal transport process in many solid-liquid nanoscale systems that contain a high density of interfaces. Experimentally, it was measured that the value of R_{SL} varies from 2×10^{-9} to 2×10^{-8} m^2 K/W depending on surface wettability [3,7]. On the other hand, molecular dynamics (MD) simulation results show that R_{SL} is a function of not only surface wettability [1,2], but also temperature, surface structure, and fluid flow rate [4–6]. Most of these MD simulations are performed in a system consisting of two solid parallel walls separated by a liquid film. None of these simulation results indicate that R_{SL} is a function of the liquid-film thickness L_F. For instance, Kim *et al.* [4] varied L_F from 3.24 to 12.96 nm, but no discernible variation of R_{SL} was observed in their simulations. In nanofluids (nanoscale colloidal suspensions), however, the separation between nanoparticle surfaces could be even smaller than the L_F used in the aforementioned simulations due to Brownian motion or aggregation of nanoparticles. In the case of particle aggregation, liquid thin films could be trapped between rough nanoparticles and could contain only a few adsorbed molecular layers. Recent theoretical and experimental studies suggested that the nanoparticle aggregating plays a significant role in the thermal transport in nanofluids [8–12]. The thermal resistance at the interface poses a barrier to heat flow through the particle clusters and affects the effective thermal conductivity of nanofluids. As the particle size decreases, the interfacial resistance may affect the nanofluids conductivity significantly [12]. The study of solid-film interfacial resistance R_{SF} is, therefore, important for understanding thermal conduction through the particle clusters in nanofluids.

As the film thickness decreases, the fraction of molecules in the thin film that is bonded to the solid atoms increases. If the film thickness is less than 1 nm, almost all liquid molecules in the film have non-negligible interactions with the solid atoms on both sides of the film. Hence, the thermal conduction across such a solid-film interface may behave differently from that across a solid-bulk liquid interface.

The solid-film interfacial resistance R_{SF} as a function of film thickness L_F is investigated in this paper by a nonequilibrium MD model. Specifically, a system consisting of an Ar thin film confined between Ag particles is employed in the simulation. The thin film in the simulation contains one to four Ar layers that correspond to film thicknesses from approximately 0.3 to 1.3 nm. For each film thickness, R_{SF} is calculated and is compared with R_{SL}. R_{SL} is obtained in a system with a film thickness that is large enough such that the interfacial thermal resistance is independent of film thickness. In the simulation, only the phonon contribution to thermal conduction is calculated since the electron transport in the system is largely suppressed by liquid Ar.

II. MD MODEL

The geometry of the system that simulates the thermal conduction through a two-particle aggregate in a liquid is depicted in Fig. 1(a). The system consists of a slab of liquid Ar at a density of 35.18 mol/L and two parallel Ag walls that sandwich an Ar thin film. Both Ag walls consist of [1 0 0]-oriented perfect fcc crystals of lengths $32a_0$ in the x direction and $8a_0$ in the y or z direction, where $a_0 = 4.086$ Å is the lattice constant of Ag [13]. The length of the liquid Ar slab is around 22 nm. Such crystal size and liquid slab length ensure that there is no statistically significant size effect on the results of the simulations [14]. Periodic boundary conditions (PBCs) are applied in three directions. The Ag-Ag interaction is modeled by the Morse potential with parameters $r_e = 3.13$ Å, $a = 1.3535$ Å^{-1}, and $D = 3775$ K [13]. The Ar-Ar interaction is modeled by the Lennard-Jones (LJ) 12-6 potential with parameters $\sigma = 3.41$ Å and $\varepsilon = 119.8$ K [15]. The LJ potential is also used to simulate the interactions between Ar and Ag. The parameters $\sigma_{Ag\text{-}Ar} = 3.12$ Å and $\epsilon_{Ag\text{-}Ar} = 204$ K are chosen so that the Ag-Ar potential reproduces the experimental data of adsorption height and energy for the Ar-Ag system [16]. The cutoff radius for all interactions
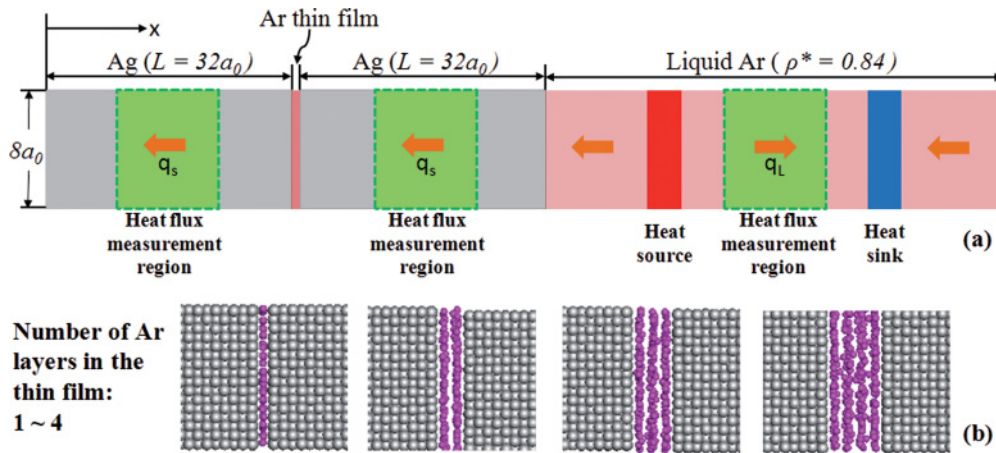
_____
[*]E-mail address: tsai@mst.edu (H.L. Tsai)

FIG. 1. (Color online) (a) The geometry of the simulation system that contains two Ag particles aggregating in liquid Ar at 150 K and 35.18 mol/L (in reduced unit $\rho* = 0.84$). The size of each Ag slab is $32a_0 \times 8a_0 \times 8a_0$ (dimensions in the figure are not to scale). The length of the liquid Ar slab is about 22 nm. PBCs are applied in three directions, (b) the Ar structures in the thin film containing different numbers of Ar layers.

is 2.5σ. Although more accurate potential models, such as three-body potentials, for Ag-Ag interactions are available, we have chosen simpler but realistic models for computational efficiency. All simulations in this paper are performed at the temperature of 150 K.

The Ar thin film should be more ordered and probably has a higher density than the bulk liquid since most Ar molecules in the thin film are in contact with the solid phase [17]. One of the important problems in the simulation, therefore, is to determine the appropriate density and structure of Ar in the thin film so that the Ar thin film confined between two Ag crystals is in equilibrium with bulk liquid Ar at 150 K and 35.18 mol/L. Figure 1(b) shows the typical structure of Ar molecules in the thin film when the number of Ar layers is 1–4. To determine the thin-film structure and density, we conduct an equilibrium MD simulation of two parallel Ag walls immersed in a liquid Ar reservoir at a temperature of 150 K and density of 35.18 mol/L. As shown in Fig. 2, the size of the Ag wall is $8a_0$ in each of the x and y directions and $16a_0$ in the z direction. The initial separation between two parallel walls is varied from σ to 4σ. Simulation systems with different initial wall separations are equilibrated for 500 ps to obtain the equilibrium structure and density of Ar between two Ag walls. We integrate the equations of motion using a velocity Verlet scheme with a time step size of 5 fs. The algorithm of Berendsen *et al.* [18] with a 0.6-ps time constant is used to equilibrate the system at 150 K. The density of liquid Ar in the reservoir is maintained at 35.18 mol/L during the equilibration. After a 500-ps equilibration period, the density distribution of liquid Ar and the distance between Ag walls become steady. The structure of Ar in the thin film shown in Fig. 1 is reproduced from the equilibrium structures of Ar in the dashed region shown in Fig. 2. As depicted in Fig. 1(b), Ar molecules in different thin-film thicknesses show layered structures. With the increase in film thickness, however, the boundaries between different Ar layers are more blurred, and the Ar structure becomes more bulklike. The solid-film interfacial resistance for each case shown in Fig. 1(b) is determined by the subsequent nonequilibrium MD simulation.

In the nonequilibrium MD simulation, each Ag solid slab is divided into 16 bins in the x direction with each bin containing four Ag atomic layers (the bin thickness is about 0.817 nm). The liquid Ar slab is divided evenly into 26 bins in the x direction (the bin thickness is about 0.882 nm). As depicted in Fig. 1(a), in the liquid Ar, bins 6–8 are set as the heat source region, and bins 19–21 are set as the heat sink region. A constant energy ΔE is added to the energy of atoms in the heat source region and is subtracted from the energy of atoms in the heat sink region at each time step by using the Jude and Jullien method [19]. Such a velocity scaling method ensures the conservation of both total energy and momentum of the system during simulation. Note the simulation system is not symmetric with respect to the heat source or heat sink. The heat fluxes flowing out from the heat source in the positive and in
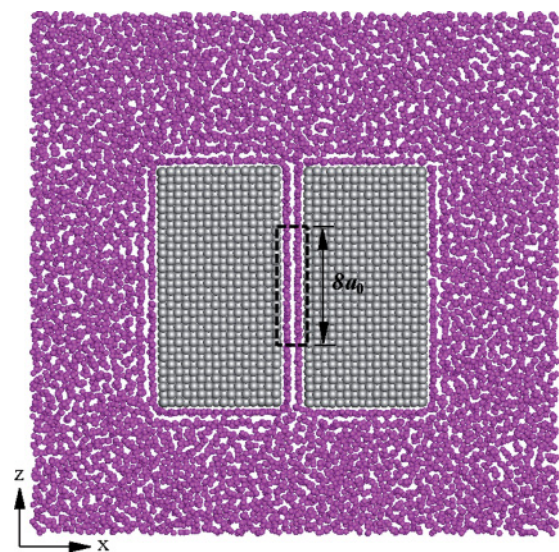

FIG. 2. (Color online) The simulation system containing two Ag planar walls immersed in a liquid Ar reservoir at 150 K and 35.18 mol/L. The Ar structure in the dashed region of length $8a_0$ is used as the initial Ar structure in the thin film shown in Fig. 1.

the negative x directions are not necessarily equal. Therefore, as shown in Fig. 1(a), the heat flux q_L in the liquid Ar and the heat flux q_S across the solid-liquid interface need to be measured during the MD simulation. Accordingly, bins 11–16 in the liquid Ar and bins 7–10 in each of the Ag regions are set as the heat flux measurement (HFM) region. To evaluate the average heat flux q in each HFM region, the following equation is used for the calculation [20]:

$$q = \frac{1}{V}\left[\sum_i E_i v_{x,i} + \frac{1}{2}\sum_i \sum_j x_{ij}^*(\vec{v}_i \cdot \vec{F}_{ij})\right]. \qquad (1)$$

In Eq. (1), V is the volume of a HFM region, E_i is the sum of the kinetic energy and potential energy of atom i, $v_{x,i}$ is the velocity of atom i in the x direction, and $\vec{F}_{ij}$ denotes the interatomic force. The first term on the right side of Eq. (1) is a summation over all atoms in the HFM region. The double summation in the second term is over all pairs of atoms with the condition that the line connecting the two atoms is contained or is partially contained in the HFM region. Accordingly, x_{ij}^* in Eq. (1) is the x component of the whole connecting vector or the portion of the connecting vector contained in the HFM region.

Before a heat source and a heat sink are applied in the simulation, a thermostat is always employed to equilibrate the system at 150 K. After a 300-ps equilibration period, the film thickness and the length of the liquid slab become stable. Based on these equilibrium values, the thickness of each bin in the liquid or solid is determined. After the equilibration period, the thermostat is removed, and a total heat flux of 0.681 GW/m² is applied to the simulation system for 3 ns to let the system reach a steady state. Subsequently, the nonequilibrium MD simulation is carried out for another 30 ns for data collection and averaging. At each time step, the temperature profile for the entire domain, including Ag solid slabs, Ar thin films and liquid Ar, and the heat flux in each HFM region, are calculated. The heat fluxes in the two solid HFM regions are found to be almost identical, as expected, and their average value is used to evaluate the heat flux across Ag-Ar interfaces. A time step size of 5 fs is employed in all simulations. Owing to the long

simulation length, the statistical uncertainties of temperature and heat flux are about ±0.2% and ±3.5%, respectively.

III. SIMULATION RESULTS

A typical temperature profile in the x direction of the simulated system is shown in Fig. 3. The results shown in Fig. 3 are obtained when there are two Ar layers in the thin film. It is seen that the temperature profiles in the two Ag solids are almost flat due to the high thermal conductivity of Ag. In the liquid Ar, the temperature profile is almost linear between the heat source and the heat sink regions. As depicted in Fig. 3, the temperature gradient in the center region of the liquid is about 2.96 K/nm. Using Eq. (1), we obtain the corresponding heat flux $q_L = 0.412$ GW/m². In this case, according to Fourier's law, the thermal conductivity of liquid Ar is 0.139 W m⁻¹ K⁻¹. This calculation result is in excellent agreement with experimental data 0.138 W m⁻¹ K⁻¹ for liquid Ar at 150 K and 35.18 mol/l [21], which validates the MD model employed in this paper.

The whole simulation system contains four Ag-Ar interfaces. The interfacial temperature difference can be observed in Fig. 3. The temperature differences at the two solid-liquid interfaces are denoted by ΔT_1 and ΔT_2 as depicted in Fig. 3. The solid-liquid interfacial resistance R_{SL} is calculated by

$$R_{SL} = (\Delta T_1 + \Delta T_2)/2q_S, \qquad (2)$$

where q_S is the heat flux measured in the solid HFM region. The same method is also applied to a system containing one, three, or four Ar layers in the thin film to determine R_{SL}. The final result of R_{SL} at 150 K is the average of the four R_{SL}'s and is found to be equal to 1.05×10^{-8} m² K/W.

The other two Ag-Ar interfaces in the simulation system are solid-film interfaces. Instead of calculating the solid-film interfacial thermal resistance R_{SF} directly using the aforementioned method, we determine R_{SF} by first calculating the thin-film thermal resistance R_F, which is defined by

$$R_F = \Delta T/q_S, \qquad (3)$$

where ΔT is the difference in solid temperatures at the solid-film interfaces as depicted in Fig. 3. In the simulation, we apply
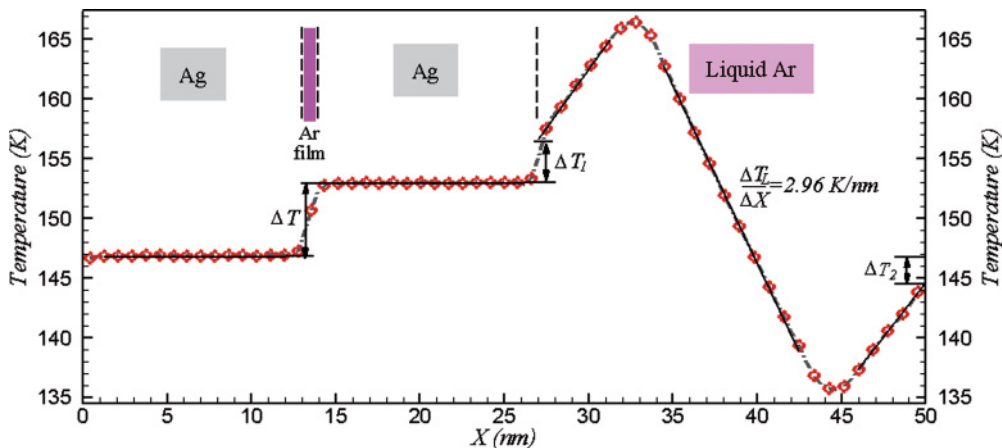

FIG. 3. (Color online) Temperature profile in the x direction of the simulated system containing two Ar layers in the thin film. ΔT_2 is determined based on the PBC in the x direction.
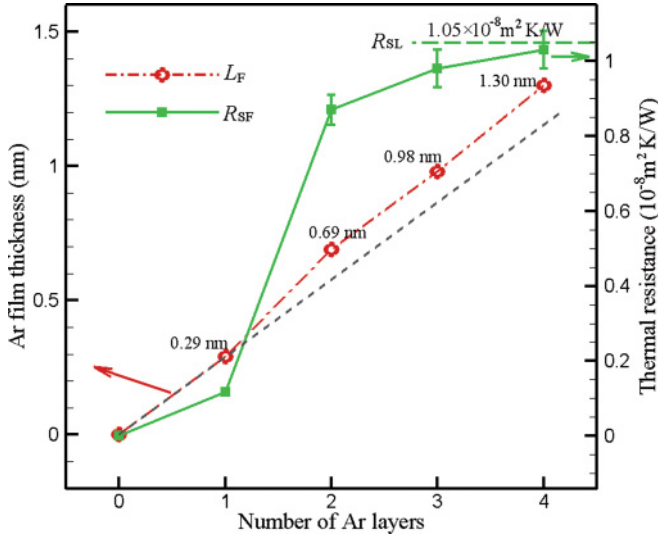
FIG. 4. (Color online) The thickness of Ar thin film L_F and solid-film interfacial thermal resistance R_{SF} as a function of the number of the Ar layers in the thin film. The dashed line shows the solid-liquid interfacial thermal resistance R_{SL}.

the method of linear least squares to the temperature profile in each Ag slab and evaluate the linear fits at the two solid-film interfaces to determine ΔT. However, the same method is not suitable for the temperature profile in the Ar thin film containing one to four Ar layers since we can only obtain very few temperature data points with relatively large uncertainties from the simulation. The few data points could result in a sizeable uncertainty in the linear fits of film temperatures at solid-film interfaces. It is the reason why we do not calculate R_{SF} directly by an equation similar to Eq. (2). To determine R_{SF}, Eq. (4), which gives the relation between R_F and R_{SF}, is employed [22] as

$$R_F = 2R_{SF} + L_F/k_F, \quad (4)$$

where L_F and k_F, respectively, represent the thickness and the thermal conductivity of the thin film. As shown in Eq. (4), the thin-film thermal resistance R_F calculated from Eq. (3) is actually the sum of R_{SF}'s at the two solid-film interfaces and the thermal conduction resistance of the thin film L_F/k_F. The thin-film thickness L_F is determined by the equilibrium MD simulation described in Sec. II. In this paper, L_F is defined by

$$L_F = x_R - x_L - a_0/2, \quad (5)$$

where x_R (or x_L) represents the x coordinate of the Ag atomic layer that is most adjacent to and on the right (or left) side of the Ar thin film. The thin-film thickness L_F, as a function of the number of the Ar layers in the film, is shown in Fig. 4. As indicated in Fig. 4, L_F does not vary linearly with the number of the Ar layer. This is because the effect of the Ag-Ar interaction on the Ar density and structure decreases as the number of the Ar layers in the thin film increases. From the calculated L_F and the number of Ar atoms in the thin film, the density of Ar in the film can readily be determined. It is found that, except for the monolayer case in which the Ar density is about 46 mol/L, the densities of other Ar thin films are all close to that of liquid Ar in the simulation system. Since the layering and ordering of liquid molecules at the solid-liquid interface has a little effect on its thermal conductivity [17,23], the thermal conductivity of the thin film k_F is assumed to be the same as that of a bulk liquid at the same density and temperature. Hence, k_F's are all equal to $0.139 W$ m^{-1} K^{-1} except that k_F in the monolayer case is equal to $0.34 W$ m^{-1} K^{-1}, which is calculated from a similar nonequilibrium MD simulation performed in a bulk liquid Ar at 46 mol/L and 150 K. Finally, the calculation results of L_F's and k_F's are used in Eq. (4) to solve for R_{SF}'s. Table I shows the simulation results in detail for each case.

Figure 4 shows the solid-film interfacial thermal resistance R_{SF} as a function of the number of Ar layers in the thin film. If there are no Ar molecules between two solid slabs and the two solid slabs are in perfect contact with each other, both L_F and R_{SF} should be zero. On the other hand, if the film thickness is large enough, R_{SF} becomes a constant and equals R_{SL}. Both of these two extreme cases are depicted in Fig. 4. We can see that all calculation results of R_{SF} are between 0 and R_{SL}. If there is only one Ar layer in the thin film, R_{SF} is found to be equal to 1.18×10^{-9} m^2 K/W, which is about 1 order of magnitude smaller than R_{SL}. While for thin films containing two or more Ag layers, R_{SF} is found to increase rapidly toward R_{SL}. The difference between R_{SL} and R_{SF} in the four-Ar-layer case is within the simulation uncertainty.

The aforementioned R_{SF}'s, which are all obtained by solving Eq. (4), require the knowledge of k_F's. Although we evaluate k_F's by assuming that the thin-film thermal conductivity is the same as that of a bulk liquid at the same density and temperature, the thermal conductivity of the thin film in the direction perpendicular to the film is actually difficult to be defined unambiguously especially for the monolayer, which makes Eq. (4), in principle, not appropriate to describe the thermal resistance of monolayer thin films. The real k_F or thermal conduction resistance of the thin film might deviate from the values shown in Table I, which will result in a different result of R_{SF}. However, as shown in

TABLE I. The simulation results for thin films containing different numbers of Ar monolayers.

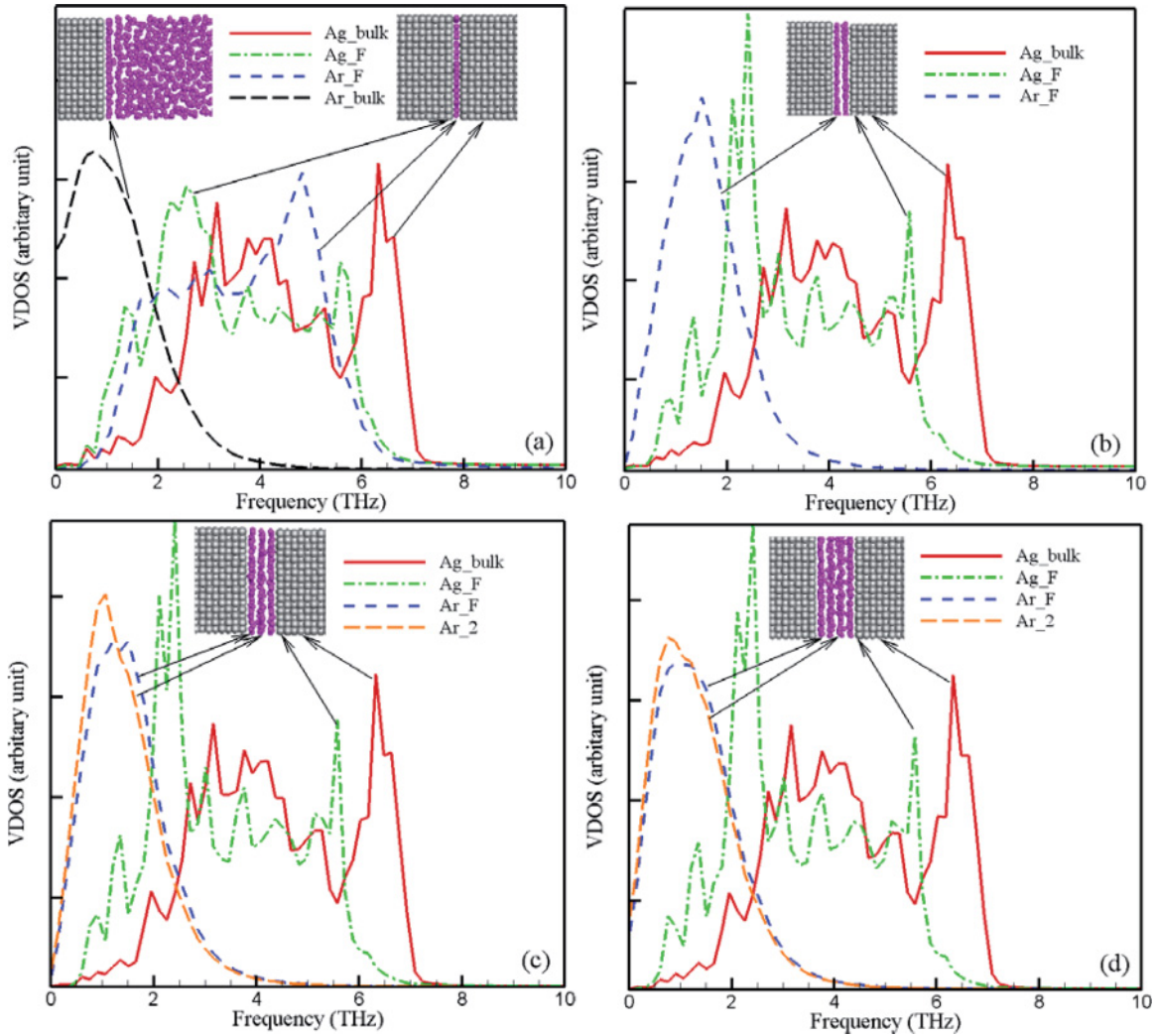| Number of layers	ΔT (K)	q_s (GW/m^2)	L_F (nm)	k_F ($Wm^{-1}K^{-1}$)	Thermal resistance (10^{-9} m^2 K/W)		
					R_F	L_F/k_F	R_{SF}
1	0.94	0.292	0.29	0.34	3.22	0.85	1.18
2	6.00	0.267	0.69	0.139	22.5	4.96	8.77
3	6.91	0.261	0.98	0.139	26.5	7.05	9.72
4	7.67	0.256	1.30	0.139	30.0	9.35	10.3

FIG. 5. (Color online) VDOS of Ag atoms and Ar molecules for thin films with different numbers of Ar layers. (a) Monolayer film, (b) two-layer film, (c) three-layer film, (d) four-layer film. Ag_bulk, Ag atoms $2a_0$ away from the thin film; Ag_F, Ag atoms in direct contact with the Ar film; Ar_F, Ar molecules in the thin film in direct contact with the Ag surface; Ar_2, Ar molecules in the thin film in the layer second closest to the Ag surface; Ar_bulk, Ar molecules in direct contact with the Ag surface in the bulk liquid.

Table I, the thin-film thermal resistance R_F's are all dominated by the solid-film interfacial thermal resistance R_{SF}. The choice of different k_F values, therefore, cannot strongly affect R_{SF}'s shown in Table I. For example, in the monolayer case if we choose a much larger k_F to make L_F/k_F approximately zero, which means only the magnitude of R_{SF} contributes to R_F. In this extreme case, the R_{SF} will be increased from 1.18×10^{-9} m^2 K/W shown in Table I to the maximum possible value of 1.61×10^{-9} m^2 K/W. This value is still significantly smaller than the solid-liquid (bulk) interfacial thermal resistance R_{SL}. On the other hand, if we choose a smaller k_F to make L_F/k_F larger, the calculated R_{SF} will be even smaller than the value 1.18×10^{-9} m^2 K/W shown in Table I. Therefore, the choice of different k_F values cannot strongly affect the general trend of R_{SF} as a function of L_F shown in Fig. 4.

To understand the mechanisms responsible for the trend of R_{SF} variations, especially the very small R_{SF} in the monolayer case, the vibrational density of states (VDOS) for

Ag atoms and Ar molecules close to the solid-film interfaces is calculated from the Fourier transform of the Ag and Ar velocity autocorrelation function [24]. The VDOS is obtained from an equilibrium MD simulation of the same system shown in Fig. 1(a) at 150 K in the microcanonical ensemble. Specifically, the VDOSs of Ag atoms in the four layers most adjacent to the solid-film interface and all Ar molecules in the thin film are calculated. The calculated VDOSs for systems with different numbers of Ar layers in the thin film are shown in Fig. 5. It is found that both Ag atoms and Ar molecules vibrate primarily with frequencies below 10 THz. Therefore, the VDOSs in the frequency range from 0 to only 10 THz are shown in Fig. 5.

As depicted in Fig. 5(a)–5(d), the VDOSs of Ag atoms in the fourth layer are all identical. While for Ag atoms at the solid-film interface, the corresponding VDOSs all show an evident shift toward the low frequency region due to the influence of the Ar thin film. The VDOSs of Ag atoms in the second and third layers (not shown) are close to those of Ag atoms in the fourth layer. Therefore, the Ar thin film has

little effect on VDOSs of Ag atoms except for those in direct contact with the thin film. As shown in Fig. 5, the VDOSs of Ar molecules strongly depend on the number of Ar layers in the thin film. When there are two or more layers of Ar in the thin film, the VDOSs mainly populate in a frequency range from 1 to 3 THz. Such VDOSs have relatively small overlaps with the VDOSs of Ag atoms, which result in a relatively large R_{SF} as compared to the monolayer film case. If only one Ar layer exists in the thin film, all Ar molecules are in direct contact with Ag atoms on both sides of the thin film. The equilibrium structure of Ag is symmetric with respect to the Ar monolayer. In this case, the vibration of Ar molecules between Ag solid slabs is analogous to a forced vibration situation in which the vibration frequency is equal to the frequency of the applied force. The force applied on Ar molecules by Ag atoms is determined by the Ag-Ar interatomic distance, which is directly related to the vibration of the Ag atoms at two surfaces. Hence, the vibration frequency of Ag atoms strongly affects the frequency of Ag-Ar interatomic forces and the vibration frequency of Ar molecules in the monolayer thin film. The VDOS of Ar molecules in the monolayer case is found to have a large overlap with that of the Ag atoms as shown in Fig. 5(a), which leads to a resonant thermal transport through the solid-film interface and results in a very small interfacial thermal resistance as shown in Fig. 4. Therefore, the liquid monolayer trapped between rough nanoparticles in nanofluids can provide additional thermal conduction paths and can enhance the heat flow among the aggregated particles.

From Fig. 5(b) to 5(d), we notice the Ar VDOSs shift slightly to the lower frequency region as the number of the Ar layers in the thin film increases. Hence, the increase in R_{SF} is observed due to the smaller overlap between the Ar and the Ag VDOSs. As shown in Fig. 5(d), the VDOS of Ar molecules has an evidently nonzero value at zero vibrational frequency when the number of the Ar layers is increased to 4. Note the VDOS at zero vibrational frequency is actually equal to three times the self-diffusion coefficient of Ar molecules in the thin film. If Ar molecules in the thin film are all confined in their molecular layers, they will vibrate around the equilibrium position and will result in a zero self-diffusion coefficient. The nonzero self-diffusion coefficient in the four-layer-film case indicates the VDOS of Ar molecules becomes bulklike. To confirm this result, we calculate the VDOS of Ar molecules that are in direct contact with the Ag surface in the bulk liquid for comparison. The results are shown in Fig. 5(a). It is seen that the VDOS distribution of Ar molecules in the four-layer-thick film is similar to that of Ar molecules in direct contact with the Ag surface in the bulk liquid. The main difference is that the VDOS at zero frequency in the bulk liquid case is larger than that in the four-layer-thick film. Therefore, it is reasonable to find that the solid-film interfacial thermal resistance R_{SF} in the four-layer-film case is close to solid-bulk liquid interfacial thermal resistance R_{SL}.

IV. CONCLUSIONS

We calculate the thermal resistance at the solid-film interface by carrying out nonequilibrium MD simulations on a system containing two Ag solids aggregating in liquid Ar. The solid-film interfacial thermal resistance R_{SF} is found to depend on film thickness if there are only a few Ar layers in the thin film. If the film contains only one molecular layer, we find that R_{SF} is about 1 order of magnitude smaller than R_{SL}. In this case, the low thermal resistance is caused by the resonant thermal transport between Ag particles and Ar thin films. Such a monolayer may provide additional thermal conduction paths and may enhance the heat flow among the aggregated particles. If there are two or more molecular layers in the film, it is shown that R_{SF} increases rapidly toward R_{SL} as film thickness increases. When there are four Ar layers in the thin film, the VDOS of Ar molecules in the thin film becomes bulklike, and R_{SF} is found to be almost identical to R_{SL}.

[1] L. Xue, P. Keblinski, S. R. Phillpot, S. U. S. Choi, and J. A. Eastman, J. Chem. Phys. **118**, 337 (2003).

[2] J.-L. Barrat and F. Chiaruttini, Mol. Phys. **101**, 1605 (2003).

[3] Z. Ge, D. G. Cahill, and P. V. Braun, Phys. Rev. Lett. **96**, 186101 (2006).

[4] B. H. Kim, A. Beskok, and T. Cagin, J. Chem. Phys. **129**, 174701 (2008).

[5] C. Liu, H. B. Fan, K. Zhang, M. F. Yuen, and Z. Li, J. Chem. Phys. **132**, 094703 (2010).

[6] D. Torii, T. Ohara, and K. Ishida, J. Heat Transfer **132**, 012402 (2010).

[7] A. J. Schmidt, J. D. Alper, M. Chiesa, G. Chen, S. K. Das, and K. Hammad-Schifferli, J. Phys. Chem. C **112**, 13320 (2008).

[8] J. W. Gao, R. T. Zheng, H. Ohtani, D. S. Zhu, and G. Chen, Nano Lett. **9**, 4128 (2009).

[9] R. Prasher, W. Evans, P. Meakin, J. Fish, P. Phelan, and P. Keblinski, Appl. Phys. Lett. **89**, 143119 (2006).

[10] R. Prasher, P. E. Phelan, and P. Bhattacharya, Nano Lett. **6**, 1529 (2006).

[11] J. Eapen, R. Rusconi, R. Piazza, and S. Yip, J. Heat Transfer **132**, 102402 (2010).

[12] W. Evans, R. Phasher, J. Fish, P. Meakin, P. Phelan, and P. Keblinski, Int. J. Heat Mass Transfer **51**, 1431 (2008).

[13] R. C. Lincoln, K. M. Koliwad, and P. B. Ghate, Phys. Rev. **157**, 463 (1967).

[14] R. J. Stevens, L. V. Zhigilei, and P. M. Norris, Int. J. Heat Mass Transfer **50**, 3977 (2007).

[15] G. C. Maitland, M. Rigby, E. B. Smith, and W. A. Wakeham, *Intermolecular Forces: Their Origin and Determination* (Clarendon, Oxford, 1981).

[16] J. Unguris, L. W. Bruch, E. R. Moog, and M. B. Webb, Surf. Sci. **109**, 522 (1981).

[17] Z. Liang and H. L. Tsai, Phys. Rev. E **83**, 041602 (2011).

[18] H. J. C. Berendsen, J. P. M. Postma, W. F. Van Gunsteren, A. Di Nola, and J. R. Haak, J. Chem. Phys. **81**, 3684 (1984).

[19] P. Jund and R. Jullien, Phys. Rev. B **59**, 13707 (1999).

[20] T. Ohara, J. Chem. Phys. **111**, 9667 (1999).

[21] E. W. Lemmon, M. O. McLinden, and D. G. Friend, *NIST Chemistry WebBook, NIST Standard Reference Database Number 69* (NIST, Gaithersburg, MD, 2010).

[22] E. S. Landry and A. J. H. McGaughey, J. Appl. Phys. **107**, 013521 (2001).

[23] L. Xue, P. Keblinski, S. R. Phillpot, S. U. S. Choi, and J. A. Eastman, Int. J. Heat Mass Transfer **47**, 4277 (2004).

[24] M. P. Allen and D. J. Tildesley, *Computer Simulation of Liquids* (Oxford University Press, Oxford, 2000).